Mine Water and the Environment (2019) 38:268–280
https://doi.org/10.1007/s10230-018-00587-w

TECHNICAL ARTICLE

Impacts of Large-Scale Rare Earth Mining on Surface Runoff, Groundwater, and Evapotranspiration: A Case Study Using SWAT for the Taojiang River Basin in Southern China

Jian Liang[1,2] · Kaixing Wu[1] · Yue Li[3] · Zhenya Wei[1,2] · Pan Zhuo[1] · Qun Yan[4] · Xianping Luo[1,2]

Received: 23 January 2018 / Accepted: 22 December 2018 / Published online: 19 February 2019

Abstract
The extensive rare earth open-pit mining in the Taojiang River basin in southern China have produced a large area of bare land during the last several decades. We assessed the effects of the bare land on surface runoff, groundwater, and evapotranspiration (ET) using the Soil and Water Assessment Tool (SWAT). A total of nine parameters were calibrated using data from 2001 to 2005 and were validated using data from 2006 to 2009, with the observed daily streamflow data as the baseline scenario. The R^2 and the Nash–Sutcliffe efficiency index ranged between 0.75 and 0.85 through the simulation periods. Moreover, two historic and four hypothetical land-use scenarios were investigated. Based on the capacity to affect surface runoff, groundwater, and ET, the ranking of land-use types was, from highest to lowest: rare earth bare land, urban land, pasture land, and forest land. Still, due to the relatively small area involved, the rare earth mining did not significantly deteriorate the local hydrological cycle from 2005 to 2015. Protecting the forest, paying attention to urban development, and enhancing infiltration in urban areas should be the top priorities in achieving sustainable development. The presented methodology provided a reliable impact assessment of the water balance components of large-scale open-pit mining activities.

Keywords Open-pit mining · Impact assessment · Water balance components · Scenario simulation · Single factor analysis

Introduction

The mining industry is the foundation of modern industry, providing most of the energy and raw materials for the global economy (Mudd 2007). The rare earth elements (REEs) are essential resources that are widely used in modern industry. REEs refers to the 15 metallic elements of the lanthanide series, coupled with the chemically similar yttrium, and occasionally scandium. These elements are typically split into two sub-groups, the cerium sub-group of "light" rare earth elements (LREEs), which includes La to Eu, and the yttrium sub-group of "heavy" rare earth elements (HREEs), which include the remaining lanthanide elements, Gd to Lu, as well as yttrium. Scandium, when it is classified as a rare earth element, is not included in either the LREE or HREE classifications (Jordens et al. 2013; Simandl 2014). The demand for REEs has spiked in recent years due to their increasing usage in numerous high-technology applications, including high strength permanent magnets, phosphors for electronic displays, applications in a variety of renewable energy technologies, and as alloying agents in metals (Gupta and Krishnamurthy 2013; Jordens et al. 2013). Each of these applications requires specific rare earth elements; the lanthanides are not interchangeable (Jordens et al. 2013).

It is said that rare earths are actually not rare. This is true for LREEs, but HREEs are much less common (Jordens et al. 2013; Kanazawa and Kamitani 2006), and are mostly mined from ion-adsorption type REE deposits (Jordens et al. 2013; Simandl 2014; Yang et al. 2013). These deposits were

✉ Qun Yan
yanqun8219893@163.com

✉ Xianping Luo
lxp9491@163.com

1 School of Resources and Environmental Engineering, Jiangxi University of Science and Technology, Ganzhou 341000, China

2 Jiangxi Key Laboratory of Environment Pollution Control of Mining and Metallurgy, Ganzhou 341000, China

3 Institute of Engineering Research, Jiangxi University of Science and Technology, Ganzhou 341000, China

4 School of Architectural and Surveying and Mapping Engineering, Jiangxi University of Science and Technology, Ganzhou 341000, China

first discovered in 1969 in Zudong, Longnan County, in southern Jiangxi Province, China. Initially, it was not considered as a mineral phase because it did not behave like any other known rare earth mineral phases. Ion-adsorption type REE deposits were formed by in situ chemical weathering of REE-rich host rocks (mainly granitoids) under conditions of prolonged weathering with limited erosion, and subsequent adsorption and enrichment onto clay minerals during the migration of rare earth mineral solutions (Gupta and Krishnamurthy 2013; Yang et al. 2013). The minerals are therefore also called weathering crust elution-deposited rare earths (Yang et al. 2013) or ion adsorption clay (Gupta and Krishnamurthy 2013; Jordens et al. 2013; Kanazawa and Kamitani 2006; Simandl 2014).

Most of the known examples of this type of REE deposit are located in southern China, especially in southern Jiangxi province, although similar deposits are found in areas with comparable climate and bedrock geology, such as Laos, northern Vietnam, Thailand, Indonesia, and Madagascar (Maulana et al. 2014; Sanematsu et al. 2013; Simandl 2014). The deposits are generally found in small mountains with a humus topsoil layer of 0.3–1 m, a full-regolith layer of 5–30 m (the main ore body, containing 0.03–0.15% REE in general), a semi-regolith layer of 2–3 m and a bedrock layer. Unlike other rare earth minerals, which are in solid state mineral phase, ion-adsorption rare earth minerals occur as an adsorbed trivalent cation that is readily extracted by a simple leaching technique with an aqueous electrolyte solution (sodium chloride or ammonium sulfate) via an ion-exchange process:

$$2(\text{Kaolin})^{3-}\text{RE}^{3+} + 3\left(\text{NH}_4\right)_2\text{SO}_4 \rightarrow 2(\text{Kaolin})^{3-}\left(\text{NH}_4\right)_3^{+} + \text{RE}_2^{3+}\left(\text{SO}_4\right)_3^{2-}.$$

Therefore, the extraction of ion-adsorption rare earths is carried out by surface/mountaintop mining followed by tank or heap leaching (Yang et al. 2013). Despite an extremely low ratio of ion-adsorption rare earth reserves (2.9% of China's total rare earth reserves), this type of rare earth accounted for 26% of China's total rare earth production between 1988 and 2007 and has reached 35% (roughly 50,000 t) since 2009 (Yang et al. 2013). Using traditional surface/mountaintop mining and heap leaching techniques, it is estimated that the production of 1 t of rare earth oxide from ion-adsorption rare earth ores entails the removal of 300 m^2 of vegetation and topsoil and the disposal of 2000 t of tailings into adjacent valleys and streams, and produces 1000 t of wastewater containing high concentrations of ammonium sulfate and metal contaminants.

Predictably, rare earth mining activities affect groundwater quantity and quality (Li et al. 2013), change land-use type (Mccullough and Etten 2011), excavate the stratum (Lai et al. 2006), disturb the hydrological cycle, and affect the whole ecosystem (Kruse et al. 2012; Palmer et al. 2010). Removal of vegetation and topsoil, the resulting changes in topography, and soil compaction reduce infiltration and storm runoff absorbing capacities, leading to increased frequency and magnitude of flooding and other geological disasters during storm periods. As a result, surface/mountaintop mining for ion-adsorption rare earth ores has become an important driver of land-use change and degradation in southern China, causing permanent loss of ecosystem, severe soil erosion, air pollution, biodiversity loss, and human health problems (Tang and Li 2000; Yang et al. 2013).

The ecosystem's vegetation landscape and land-use type affect hydrological processes such as precipitation interception, evapotranspiration (ET), rainfall infiltration, groundwater recharge, and surface runoff (Kundu et al. 2017). The vegetation deterioration and land-use change caused by mining activities inevitably change the local hydrological conditions and modify surface runoff, groundwater, and ET (Poff and Zimmerman 2010).

Human activities and land-use and cover change (LUCC) impact the hydrological cycle (Li et al. 2017; Wu et al. 2017). The Soil and Water Assessment Tool (SWAT) is an eco-hydrological model with a strong physical basis (Griensven et al. 2006) that simulates the process of rainfall-runoff, sediment yield, and pollutant-nutrient transportation at different basin scales (White et al. 2011). SWAT was invented by the U.S. Dept. of Agriculture (USDA) in the early 1990s and has now been extensively used for assessing water resources (Baker and Miller 2013; Can et al. 2015; Jayakrishnan et al. 2005; Narsimlu et al. 2013), tackling water environment challenges (Abbaspour et al. 2007; Jha et al. 2007; Ng et al. 2010), and finding alternative water management solutions (Kaur et al. 2003; Saha and Zeleke 2015; Volk et al. 2016) all over the world.

As mentioned above, the first ion-adsorption type REE deposit was discovered in Zudong in this area in 1969, and this area has been mined ever since (Ruan et al. 2012). The original forest has been transformed into bare land in and around the mining area. Based on the SWAT model and the single factor scenario analysis method, we chose the Taojiang River basin to: (1) assess the impacts of LUCC and large-scale rare earth mining activities on the water balance components during the last decade, and (2) find reliable guidelines for the sustainable development of the Taojiang River basin.

Materials and Methods

Study Area

The Taojiang River basin (24°29′–25°54′N, 114°10′–115°19′E) covers an area of 7861 km^2 and is located in the south of the Jiangxi Province, China. The Taojiang River rises in the Jiulian Mountains, which is the junction of the Jiangxi and Guangdong provinces, flows from southwest to northeast and feeds the Ganjiang River, which is a tributary of the Yangtze River (Fig. 1). The mainstream length of the Taojiang River is 272 km and the annual average runoff is 55×10^8 m^3. The elevation of the Taojiang River basin ranges from 59 to 1391 m, averaging 484 m.

The Taojiang River basin is dominated by a subtropical monsoon climate. The average annual temperature is about 19.9–20.9 °C, the mean annual humidity is around 75%, and the mean annual number of rainy days is approximately 200 days. The annual average precipitation ranges from 1400 to 1800 mm, 50–60% of which occurs from April to July. The streamflow of the Taojiang River varies significantly by season due to the interaction of the high solar radiation and monsoon weather patterns. Thus, this area frequently suffers from flooding during the monsoon period.

The southern Jiangxi Province is located in the central Nanling Range in the Cathaysia Block, where the basement is composed of 1.9–1.8 Ga sedimentary rocks and Neoproterozoic to Early Paleozoic metamorphic rocks. Due to the early Paleozoic (Caledonian) orogeny, late Ordovician to middle Devonian strata are absent (Hu and Zhou 2012), and thus the metamorphosed basement is overlain unconformably by the late Devonian to Triassic strata marine sedimentary cover. A profound feature of south China is the giant Mesozoic igneous province, which forms a swath more than 1300 km wide across the whole Cathaysia Block and the eastern part of the Yangtze Block (Li and Li 2007). The granitic rocks in this province range in age from Jurassic to Cretaceous, notably the early (180–125 Ma) and late (110–85 Ma) Yanshanian periods. These igneous rocks were probably formed by the westward subduction of the Pacific oceanic lithosphere beneath the Eurasian continent (Hu and Zhou 2012). It is noteworthy that the Yanshanian granitoids are not only associated with the world-class W-Sn-Nb-Ta mineralization (Chengyou et al. 2012; Hu and Zhou 2012; Mao et al. 2013) but are also the main parent rocks of the HREE ore deposits (Bao and Zhao 2008; Ishihara et al. 2010; Wu et al. 1990; Yang et al. 2013).

Unlike the upper part of the Taojiang River basin, which is mountainous, the middle and lower reaches is hilly, except for the plain distributed in the two Cretaceous red basins in Longnan and Xinfeng Counties. The exposed strata in the basin are mainly composed of folded basement (Z-O), marine sedimentary cover (D-T1), Cretaceous red layer (K2), and Quaternary (Q) (Fig. 1). The quaternary system (Q) is distributed along the Taojiang River valley and its

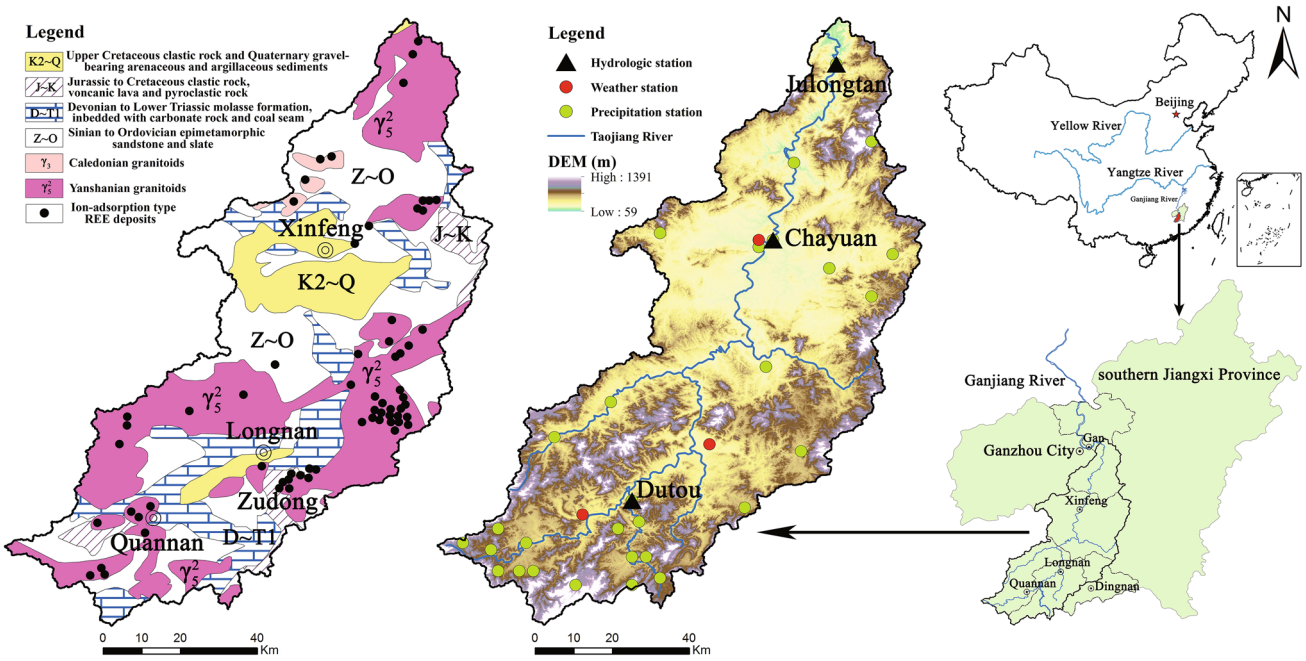

Fig. 1 Geological map (left), elevation map (middle), and geographical map (right) of the Taojiang River basin

tributaries. The Cretaceous red clastic rocks (K2) are mainly distributed in the syncline basins in the Quannan, Longnan, and Xinfeng counties. The sedimentary cover (D-T1), composed of neritic molasse formation, embedded with carbonate rock and coal seams, were bands or islands on the edge of the basin. The folded basement (Z-O) is originally a thick sub-flysch formation, which metamorphosed into epimetamorphic sandstone and slate.

Extensive Yanshanian granitoids, as well as minor Caledonian ones, intruded into the folded basement and outcropped at the low mountains and hills around the red basins in the Taojiang River basin, they cover 2644.8 km^2 or 33.65% of this total area. Coupled with the moderate undulating temperature, the warm and humid climate caused the strong chemical weathering of the granitoids, which led to a well-developed weathering crust with a thickness of up to 40 m. As a result, a large number of HREE deposits, including the well-known Zudong deposit, formed in the basin (Bao and Zhao 2008; Ishihara et al. 2010; Wu et al. 1990; Yang et al. 2013; Zhang et al. 2015). The granitic weathering crust is loose sandy soil, mainly composed of clay and quartz; therefore, once the surface vegetation is peeled off by human activities, it can easily be eroded away.

Data

Key SWAT input data include daily climate and precipitation data, daily streamflow data, and the digital elevation model (DEM), land-use map, and soil map (Table 1). Three weather stations, 29 precipitation gauges, and three streamflow monitoring stations exist within the basin (Fig. 1). Daily streamflow data were acquired from 2001 to 2009 from the three streamflow monitoring stations to test the SWAT model during the baseline simulation periods.

Daily meteorological data (1960–2015) were processed into average monthly statistics to create the SWAT weather generator for the study area. Daily maximum and minimum air temperature, relative humidity, solar radiation, and wind speed measurements were obtained from the three climate stations. Daily precipitation measurements from the 29 gauges (Fig. 1) were also used for the SWAT simulations.

Land-use types were reclassified into eight categories: rare earth bare land (BARE), urban land (URBN), pasture land (PAST), forested land (FRST), agriculture land (AGRL), rice paddies (RICE), water (WATR), and wetland (WETL). BARE (Fig. 2) was separated out and simulated using the barren crop parameters provided with the SWAT model. Detailed land-use maps are shown in Fig. 2 for 2005, 2010, and 2015. This was used as the basis for the baseline scenario and two historical land-use scenarios presented below.

SWAT Model Setup

The SWAT simulated the main hydrological processes: precipitation, evaporation, infiltration, surface runoff generation, and aquifer recharge (Li et al. 2015). The basin hydrological cycle (simulated by the SWAT) can be separated into two major phases: (1) the land phase and (2) the water routing phase. The land phase determines the quantity of water input. The water routing phase simulates water movement along the stream channel network; this network, which interconnects numerous sub-basins, was derived based on topography. Sub-basins were then divided into hydrological response units (HRUs) with unique land-use, soil, and slope characteristics. The runoff produced in each HRU was calculated and summed up with others in the same sub-basin. It was then routed to the corresponding reaches and to the basin outlet along the stream channel network, which contained ponds and reservoirs (Arabi et al. 2008).

ArcSWAT version 2012.10_1.18 was used in this research; it is one of the major releases of SWAT version 2012 (SWAT2012). The basin was divided into 27 sub-basins (and 327 HRUs) based on eight land-use types, 27 soil classes, and four slope classes (0–3%, 3–5%, 5–8%, and > 8%). This discretization considered the original distribution of land-use, soil, and slope, while keeping a reasonable number of the HRUs. Meteorological data, land-use

Table 1 Key input data used to test the SWAT model for the Taojiang River basin

Data	Resolution	Source
Climate	3 stations (Fig. 1)	The China Meteorological Data Sharing Service System website (http://data.cma.cn)
Precipitation	29 gauges (Fig. 1)	Hydrological data yearbook of The People's Republic of China
Streamflow	3 stations (Fig. 1)	Hydrological data yearbook of The People's Republic of China
Digital Elevation Model (DEM) map	30 m (Fig. 1)	Geospatial Data Cloud site, Computer Network Information Center, Chinese Academy of Sciences (http://www.gscloud.cn)
Land-use map	30 m (Fig. 2)	Data Center for Resources and Environmental Sciences, Chinese Academy of Sciences (RESDC) (http://www.resdc.cn)
Soil map	1000 m	Harmonized World Soil Database (HWSD, v1.2) (http://webarchive.iiasa.ac.at)

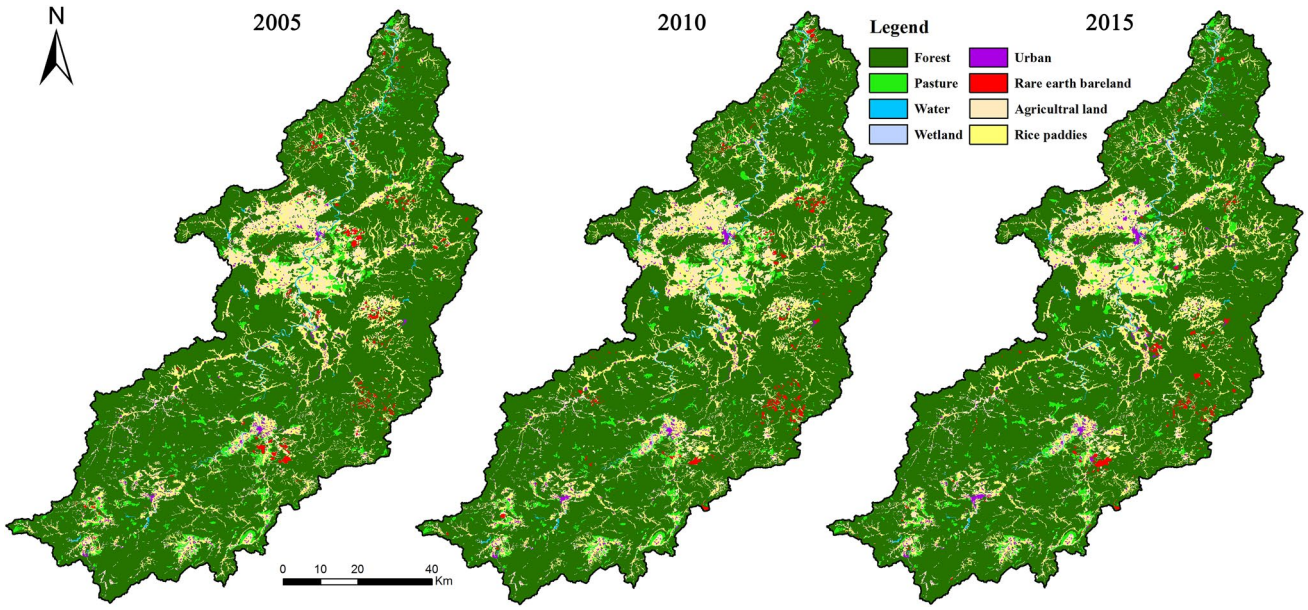

Fig. 2 Land-use maps of the Taojiang River basin for 2005 (left), 2010 (middle), and 2015 (right)

properties, and soil databases were edited and processed into the model to provide the required data for the study area.

Generally, testing of the SWAT and other similar models was performed by dividing the observed data into two groups based on time periods: one for calibration and another for validation. The calibration process was divided into two steps (Arnold et al. 2012): (1) basic water balance and total flow calibration, and (2) temporal flow calibration. The SWAT model used a series of parameters to describe the complicated hydrological characteristics of the modeled basin. During the calibration stage, a baseflow filter program (Arnold and Allen 1999) was used to calculate the proportion of groundwater and surface components vs the total streamflow, making use of the observed daily streamflow records. To ensure the accuracy and promote the efficiency of the process, a hybrid method was adopted during the calibration process. This was followed by manually specifying a parameter value or range. Then the SWAT-CUP (version 5.1.6.2) software was used to employ a sequential uncertainty fitting algorithm (SUFI-2) and Latin hypercube sampling one-at-a-time (LH-OAT), in order to conduct an automatic calibration and sensitivity analysis (Jung et al. 2010; Wu and Chen 2015).

The year 2000 was chosen as a warm-up period to initialize the model parameters and reach a reasonable value. Historical streamflow data from 2001 to 2005 were the used for calibration, and data from 2006 to 2009 were used for validation. Because SWAT is a deterministic model with a strong physical foundation, the output results are changeless while the input data is constant (Mccarty et al. 2016). Then the single factor scenario analysis method, which fixed other factors and only changed the land-use type data, was employed to study the relative changes of the certain results between each scenario. Figure 3 shows a typical flow chart of the calibration, validation, and scenario setting process (Zhang et al. 2011).

Model Evaluation Method

The competence of the SWAT used in the study area was indicated by the determination coefficient (R^2), the Nash–Sutcliffe efficiency coefficient (NSE), and the percent bias (PBIAS) (Gyamfi et al. 2016). The R^2 (which ranges from 0 to 1) is the square of the correlation coefficient and indicates the

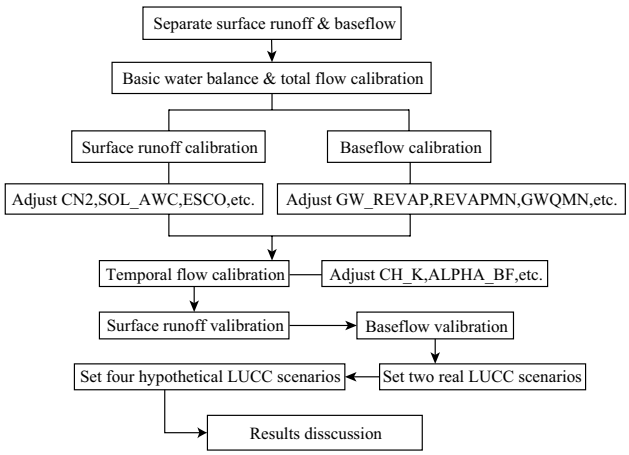

Fig. 3 Flowchart of the calibration, validation, and scenario setting process

consistency between the observed and simulated values. The R^2 is calculated as:

$$R^2 = \frac{\left[\sum_{i=1}^{n}\left(Q_{obsi} - Q_{obsave}\right)\left(Q_{simi} - Q_{simave}\right)\right]^2}{\sum_{i=1}^{n}\left(Q_{obsi} - Q_{obsave}\right)^2 \sum_{i=1}^{n}\left(Q_{simi} - Q_{simave}\right)^2}. \quad (1)$$

A weakness of using the R^2 statistical indicator is that the R^2 value can come close to 1 due to systematic over- or under-prediction. To accurately evaluate the performance of the SWAT model, the NSE (ranging from -∞ to 1) was presented. A recent study suggested that the NSE needed to be larger than 0.50 to estimate streamflow in basin scales (Moriasi et al. 2015). The Nash–Sutcliffe coefficient (NSE) is calculated as:

$$NSE = 1 - \frac{\sum_{i=1}^{n}\left(Q_{simi} - Q_{obsi}\right)^2}{\sum_{i=1}^{n}\left(Q_{obsi} - Q_{obsave}\right)^2}. \quad (2)$$

The PBIAS indicates the average deviation degree of the simulated results from the observed data. The optimal PBIAS value is 0, with lower absolute values indicating a more accurate model performance. Positive and negative PBIAS values indicate under- or over-estimation bias, respectively. PBIAS is calculated as:

$$PBIAS = \frac{\sum_{i=1}^{n} 100\left(Q_{obsi} - Q_{simi}\right)}{\sum_{i=1}^{n} Q_{obsi}}, \quad (3)$$

where n is the number of time steps; Q_{obsi} and Q_{simi} is the observed and simulated streamflow at time step i; and Q_{simave} and Q_{obsave} is the average simulated and observed streamflow across all the time steps.

Description of LUCC Scenarios

Table 2 shows the proportions of land-use change for each scenario including the eight land-use classes. This study investigated six different LUCC scenarios to assess the impacts of rare earth mining on the hydrology of the river basin (Table 2). The six scenarios included two historical scenarios (2010 and 2015) and four hypothetical scenarios. These hypothetical scenarios are rare earth bare land (BARE) entirely converted to (1) urban land (URBN), (2) pasture land (PAST), and (3) forested land (FRST), respectively, and (4) rare earth mines entirely dedicated to mining. The use of two historical scenarios investigated the tendency of LUCC during the last decade. The goal of the first three hypothetical scenarios was to determine the hydrological impact rank of the different dominant land-use types. The last scenario was an extreme scenario used to quantify the maximum hydrological impacts of overall rare earth mining activities in the Taojiang River basin.

To ensure the reliability and accuracy of the model's results, the calibrated parameters, meteorological data,

Table 2 The area and percentage of land-use types that were simulated in different scenarios

Land-use type	BARE	URBN	PAST	FRST	AGRL	RICE	WATR	WETL
Baseline (historical, 2005)								
Area (km^2)	66.3	82.1	247.2	6072.5	525.1	816.6	42.3	8.6
Percentage (%)	0.84	1.04	3.14	77.25	6.68	10.39	0.54	0.11
Scenario 1 (historical, 2010)								
Area (km^2)	63.9	85.2	247.9	6066.7	527.6	817.9	42.7	8.6
Percentage (%)	0.81	1.08	3.15	77.18	6.71	10.40	0.54	0.11
Scenario 2 (historical, 2015)								
Area (km^2)	54.7	101.7	274.6	6039.3	525.6	813.4	42.7	8.6
Percentage (%)	0.70	1.29	3.49	76.83	6.69	10.35	0.54	0.11
Scenario 3 (hypothetical)								
Area (km^2)	0	148.3	247.2	6072.5	525.1	816.6	42.3	8.6
Percentage (%)	0	1.89	3.14	77.25	6.68	10.39	0.54	0.11
Scenario 4 (hypothetical)								
Area (km^2)	0	82.1	313.4	6072.5	525.1	816.6	42.3	8.6
Percentage (%)	0	1.04	3.99	77.25	6.68	10.39	0.54	0.11
Scenario 5 (hypothetical)								
Area (km^2)	0	82.1	247.2	6138.7	525.1	816.6	42.3	8.6
Percentage (%)	0	1.04	3.14	78.10	6.68	10.39	0.54	0.11
Scenario 6 (hypothetical)								
Area (km^2)	2644.8	66.4	182.9	3910.5	404.1	614.1	30.7	7.0
Percentage (%)	33.65	0.84	2.33	49.75	5.14	7.81	0.39	0.09

BARE rare earth bareland, *URBN* urban land, *PAST* pasture land, *FRST* forest land, *AGRL* agriculture land, *RICE* rice paddies, *WATR* water, *WETL* wetland

landscape characteristics, and soil data used for the baseline simulation were also used for the six scenarios. This provided a consistent comparison between the baseline and the six LUCC scenarios for the simulation period of 2001–2009, which was also the time period used for the baseline model.

Scenarios 1 and 2 are the actual land-use conditions for 2010 and 2015, respectively, based on the land-use maps for those 2 years (Fig. 2). Remote sensing data indicated that land-use changes in the river basin occurred at a moderate rate, resulting in a continuous decrease in rare earth bare land. First, it decreased slightly from 0.84 to 0.81% between 2005 and 2010; then, it decreased from 0.81 to 0.70% between 2010 and 2015. The total forest land area also decreased from 77.25 to 77.18% between 2005 and 2010; and then from 77.18 to 76.83% between 2010 and 2015. The total pasture area followed the opposite pattern, increasing from 3.14 to 3.15% between 2005 and 2010, and further increasing from 3.15 to 3.49% between 2010 and 2015. Agricultural land and rice paddy areas increased slightly from 6.68 to 6.71% and from 10.39 to 10.40%, respectively, between 2005 and 2010; they then decreased slightly from 6.71 to 6.69% and from 10.40 to 10.35%, respectively, between 2010 and 2015. The remote sensing data further suggested that the total proportion of urban area gradually expanded from 1.04 to 1.29% between 2005 and 2015. The proportion of urban area increased at approximately 0.01% annually from 2005 to 2010, and then increased at approximately 0.04% annually from 2010 to 2015.

In order to seek further insight into the impacts of rare earth mining activities on the Taojiang River basin's water budget, four hypothetical scenarios (scenario 3–6) were proposed. Scenarios 3–5 represent three hypothetical scenarios that compared the influence of rare earth bare land and other dominant land-use types on the water budget. Specifically, the total rare earth bare land was completely changed to urban land (scenario 3), pasture land (scenario 4), or forest land (scenario 5) in each scenario (Table 2). To account for potential impacts of "extreme" rare earth mining activity on the basin's water budget, the granitoid area (2644.8 km^2) (Fig. 1) was completely converted to rare earth mining area in scenario 6. This increased the area of rare earth bare land from 66.3 to 2644.8 km^2, and the increased the percentage from 0.84 to 33.65%.

Results and Discussion

Parameters Calibration Results

Table 3 displays the sensitivity rank of the SWAT model parameters during the calibration process. The most sensitive parameter is the initial curve number for moisture condition II (CN2). Surface runoff in the SWAT is calculated using a modified Soil Conservation Service (SCS) curve number (CN) equation, which considers precipitation, land-use, and soil conditions (Lee et al. 2014). The CN2 value reflects the basin characteristics before rainfall, and this indicates that the parameter is important for calculating surface runoff (Feyereisen et al. 2007). Similar results were reported in a previous study that showed that the most sensitive parameters controlling surface runoff and groundwater recharge were CN2 and GWQMN, respectively (Kushwaha and Jain 2013).

SWAT Performance

The simulated and observed daily streamflow data from 2001 to 2005 (calibration period) and from 2006 to 2009 (validation period) from the three gauging stations are shown in Fig. 4. Although the model obviously underestimated the peak value during the wet season, and overestimated streamflow during several time periods in the dry season, it worked well overall for the entire simulation period. The R^2 and the NSE exceeded 0.80 in all three gauges during the calibration period, and the corresponding R^2 and NSE values exceeded 0.75 during the validation period (Fig. 4; Table 4).

Table 3 The sensitivity rank of model parameters

Parameter	Definition	Unit	Rank	Calibrated result
CN2	Initial SCS runoff curve number for moisture condition II	Dimensionless	1	Multiply original values by 0.86
GWQMN	Threshold depth of water for occur return flow	mm H_2O	2	415.32
ESCO	Compensation factor for soil evaporation	Dimensionless	3	0.06
SOL_AWC	Available water capacity of the soil layer	mm H_2O/mm soil	4	Multiply original values by 0.97
ALPHA_BF	Groundwater recharge alpha factor	1/days	5	0.07
CH_K2	Effective hydraulic conductivity for main channel alluvium	mm/h	6	53.93
GW_REVAP	Groundwater re-evaporation coefficient	Dimensionless	7	0.04
CH_K1	Effective hydraulic conductivity for tributary channel alluvium	mm/h	8	48.68
REVAPMN	Water threshold depth in the shallow aquifer for occur re-evaporation	mm H_2O	9	265.73

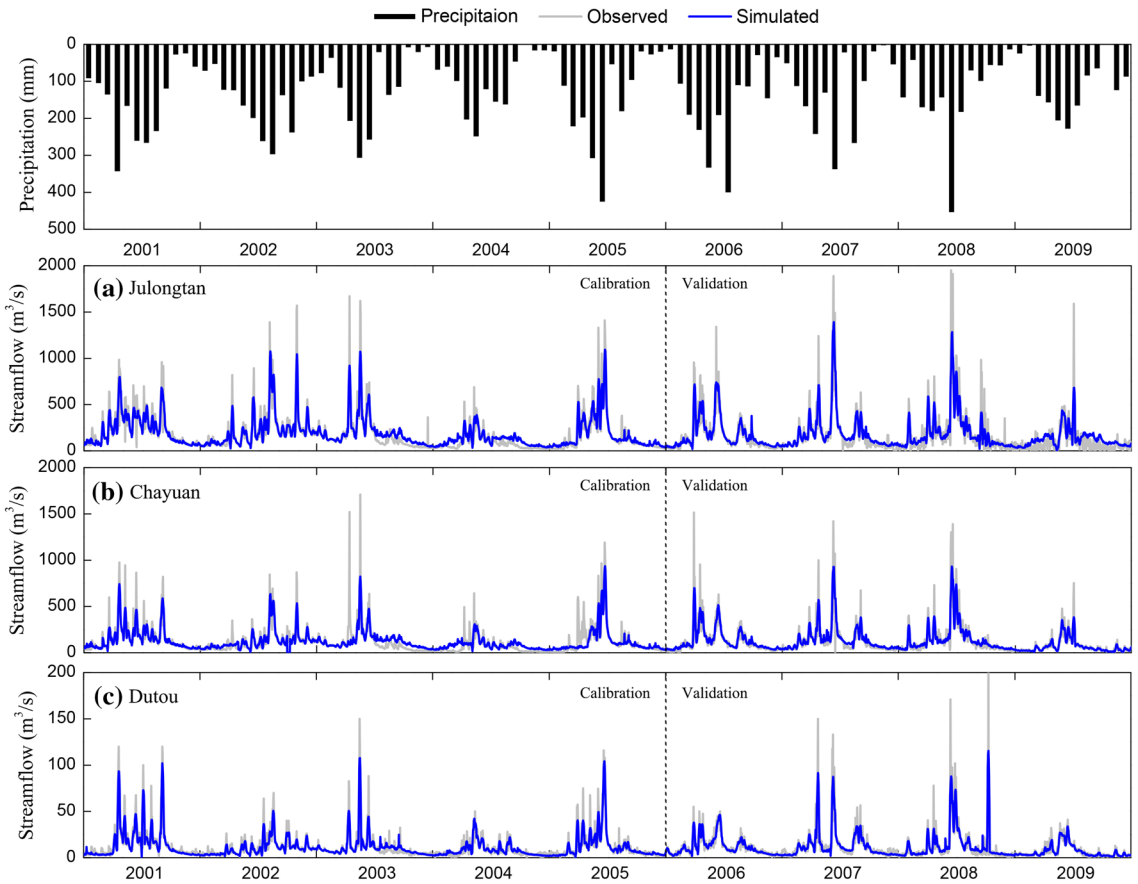

Fig. 4 Precipitation and daily streamflow results during the simulation periods at the Taojiang River basin from the **a** Julongtan, **b** Chayuan, and **c** Dutou hydrological station

According to the performance evaluation criteria recommended by Moriasi et al. (2015), this equates to "Good" performance. All of the absolute PBIAS values were computed to be less than 10% across the entire simulation period (Fig. 4; Table 4), and the negative PBIAS values mean that the estimated values were generally slightly greater than the observed values. The results indicate that the calibrated model can be used to predict streamflow during the simulation period, and to analyze the relationship between LUCC and the Taojiang River basin's water balance.

The probable cause of the model error is the inhomogeneous space-temporal distribution of precipitation within the year, due to the huge elevation difference of the study area and the sub-tropical monsoon climate. Notice that peak runoff typically occurred in a day when the runoff was far greater than in adjacent days. The model did not replicate the peak runoff, possibly because the weather and precipitation stations were not uniformly distributed, and failed to capture the short-term torrential rain that caused the flood.

Hydrological Response to Real LUCC Scenarios

The hydrological impacts of the two real LUCC scenarios are shown as plots of average monthly surface runoff,

Table 4 Statistical results of model simulation periods

Hydrological station	Calibration (2001–2005)			Validation (2006–2009)		
	R^2	NSE	PBIAS	R^2	NSE	PBIAS
Julongtan	0.85	0.83	−3.7	0.79	0.79	−5.4
Chayuan	0.82	0.81	−4.5	0.79	0.78	−6.1
Dutou	0.81	0.80	−7.8	0.76	0.75	−9.4

The determination coefficient (R^2), the Nash–Sutcliffe efficiency coefficient index (NSE), and the percent bias (PBIAS)

groundwater recharge, and ET from 2001 to 2009 (Fig. 5). It is also shown in the average monthly values of the same three water balance components in Table 5 for the baseline and two historical scenarios (2010 and 2015). The plots of the water balance components in Fig. 5 revealed that very slight impacts in water balance were predicted between the 2005 baseline and the 2010 historical land-use (scenario 1), and that somewhat larger impacts occurred between the 2005 baseline and 2015 (scenario 2). Based on the monthly averages listed in Table 5, the scenario 1 surface runoff increased 0.08%, groundwater recharge decreased 0.05%, while ET decreased 0.04% relative to the baseline.

Larger impacts were predicted for scenario 2: a 0.16% increase in the surface runoff, a 0.11% decrease in the groundwater recharge, and a 0.13% ET decrease between the baseline and scenario 2. These results are consistent with existing research showing that moderate land-use changes produced minor changes in the water budget.

Because of measures to control rare earth exploitation, production, and export, as well as the local government's attention to the ecological environment of the mines, the scale of rare earth mining has been continuously decreasing during the last decade (2005–2015) in the Taojiang River basin, despite the increased price and demand for REEs. The rare earth bare land area decreased from 66.3 to 54.7 km^2, and the area proportion decreased from 0.84 to 0.70%. Meanwhile, the rapid expansion of the local economy has led to fast expansion of the cities. The urban area increased from 82.1 to 101.7 km^2, and the area proportions increased from 1.04 to 1.29%, with an annual increase rate of about 0.01% and 0.04% for the first and second half of the last decade, respectively. Meanwhile the forest area decreased from 6072.5 to 6039.3 km^2, and the area proportion decreased from 77.25 to 76.83%, with an annual decrease rate of about 0.02% and 0.07% for the first and second half of the last decade, respectively. The areas and proportions of the other dominant land-use types were unchanged (Table 2).

Table 5 Simulated average monthly water balance components for historical scenarios at the Julongtan hydrological station for 2001–2009

Scenarios	Surface runoff (mm)	Groundwater recharge (mm)	Evapotranspiration (mm)
Baseline	38.06	18.75	55.63
Scenario 1	38.09	18.74	55.61
Scenario 2	38.12	18.73	55.56

The rare earth mining activities has had an important impact on the hydrological cycle for the Taojiang River basin. The increase in surface runoff shown in Fig. 5 for scenario 1 is attributed mainly to the decrease in forest area between 2005 and 2010. Similar impacts are implied by the even stronger responses predicted for scenario 2 (2015 land-use), during which the urban area proportion increased at a rate of 0.04% per year, while the mining area proportion

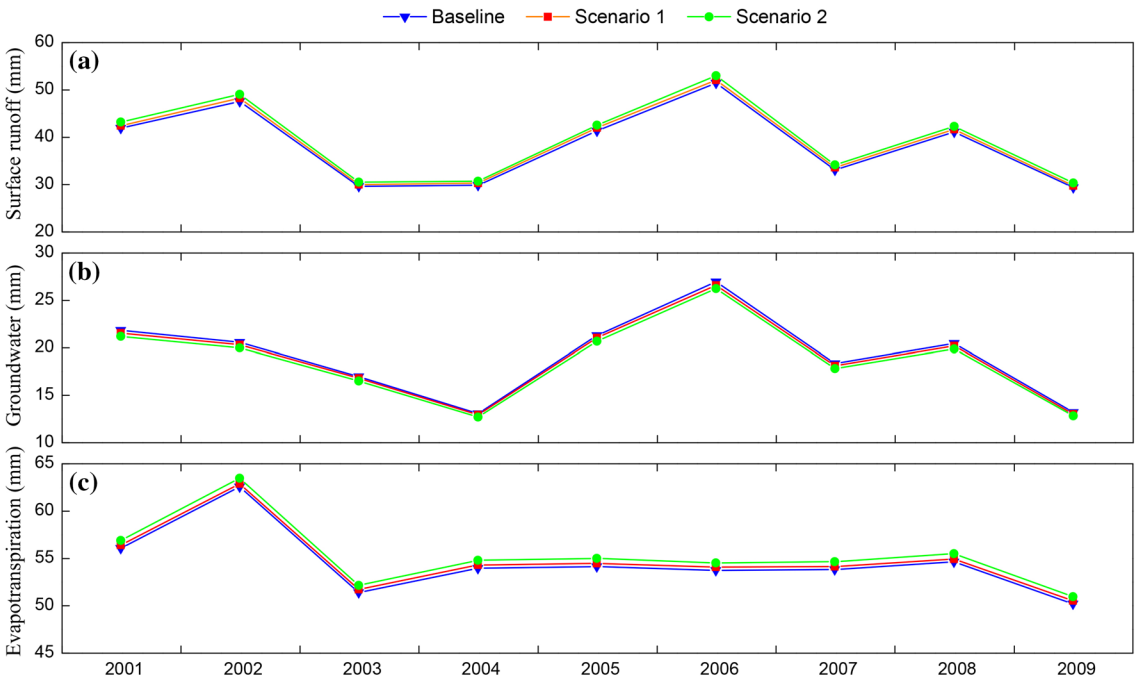

Fig. 5 Comparison of main water balance components between the baseline scenario and scenarios 1–2 for **a** surface runoff, **b** groundwater recharge, and **c** evapotranspiration

decreased at a rate of 0.02% per year and the forest area proportion decreased at a rate of 0.07%. Thus, the increase in surface runoff (Fig. 5) for scenario 2 is attributed mainly to the loss of forested land and the urban expansion between 2010 and 2015.

Due to the decrease in mining activities, updates of mining techniques, and contemporaneous reclamation practices, the rare earth bare land has continued to decrease during the last decade. The rapid development of urban land and continuing decrease of forested land is responsible for an overall deterioration of the Taojiang River basin's water budget, with an increased surface runoff and decreased groundwater recharge and ET.

Hydrological Response to Hypothetical LUCC Scenarios

Figure 6 graphically compares the average monthly water balance components over the 2001–2009 simulation period for the baseline and hypothetical LUCC scenarios (scenarios 3–6). The long-term average monthly values of water balance components for the baseline and hypothetical scenarios are listed in Table 6.

The predicted impacts were generally linear relative to the baseline levels (Fig. 6). Based on the long-term average monthly values shown in Table 6, surface runoff decreased by 0.16%, 0.37%, and 0.58%; groundwater recharge increased by 0.27%, 0.43%, and 0.64%; and ET increased 0.27%, 0.31%, and 0.65% from baseline to scenario 3, 4, 5, respectively.

Table 6 Simulated average monthly water balance components under hypothetical scenarios at the Julongtan hydrological station

Scenarios	Surface runoff (mm)	Groundwater recharge (mm)	Evapotranspiration (mm)
Baseline	38.06	18.75	55.63
Scenario 3	38.00	18.80	55.78
Scenario 4	37.92	18.83	55.80
Scenario 5	37.84	18.87	55.99
Scenario 6	45.96	15.19	42.24

It is evident that the forest land has the strongest water-holding and evaporation capacity, and that bare land has the weakest water holding and evaporation capacity. Therefore, the rank for negative hydrological impacts for the four main land-use types is, from highest to lowest: BARE, URBN, PAST, and FRST.

The total conversion of the granitoid area to rare earth bare land (scenario 6) resulted in a surface runoff increase of 20.76%, a groundwater recharge decrease of 18.99%, and an ET decrease of 24.07% (Table 6; Fig. 6). This reveals the potential maximum hydrological impact of an "extreme" rare earth mining scenario. The hypothetical results for scenarios 3–5 (Table 6; Fig. 6) showed smaller

Fig. 6 Comparison of main water balance components between the baseline scenario and scenarios 3–6 for **a** surface runoff, **b** groundwater recharge, and **c** evapotranspiration

Table 7 Simulated average annual streamflow under different scenarios at the Julongtan hydrological station

Scenarios	Baseline	Scenario 1	Scenario 2
Streamflow ($m^3\ s^{-1}$)	170.31	170.42	170.54

hydrological impacts predicted than the historical changes in scenarios 1 and 2 (Table 5; Fig. 5).

By comparing the scenario 3–5 results, it can be inferred that forested and pasture land amplify soil infiltration, resulting in less surface runoff and more groundwater recharge than urban land and rare earth bare land. The decrease in ET is due to the decreased vegetative cover area, which results in decreased transpiration.

Table 7 showed that streamflow increased slightly in the Taojiang River basin during 2005–2015. However, the two historical scenarios (scenarios 1 and 2; Table 5; Fig. 5) showed that the overall trend of surface runoff increased due to the combination of rare earth mining activities, urban development, and forest degradation; this also indicates that the ecological environment had deteriorated.

Combined with the discussion pertaining to hypothetical scenarios 3–5 (Table 6; Fig. 6), it can be inferred that rare earth bare land exerts the most severe hydrological impact; it produced the most surface runoff, the least groundwater recharge, and the least ET. The rare earth mining technology removes the vegetative cover and top soil. The bare land surface was hard and dense after mining, and the porosity was less than the original soil surface. This means that the precipitation that falls onto this area has difficulty infiltrating into the soil profile and tends to produce more surface runoff than groundwater recharge.

Although the urban land has a larger scale of impermeable surfaces (such as waterproof roofs and cement pavements), the greenbelt along the roads, the green zones, and the parks scattered in the urban cities provide considerable urban green space. Compared to bare land, urban land intercepted and collected more precipitation to infiltrate the soil profile, had greater ET, and provided more groundwater recharge.

Unlike urban land, which contains considerable impermeable interfaces, pasture and forested land are covered with vegetation all year round. The surface soil is rich in roots and is loose and, thus, precipitation easily infiltrates. Transpiration by the vegetation that grows in these two types of land-use constantly transfers water from the soil and groundwater to the external environment. Thus, pasture and forest land produces less surface runoff, more groundwater recharge, and more ET than urban land. In addition, forested land has greater vegetation coverage, bigger leaf areas, and deeper root growth depth than pasture land, and therefore, produces less surface runoff, more groundwater recharge, and more ET.

These conclusions derived from the hypothetical scenarios are consistent with previous research from different areas across the world (e.g. Hua et al. 2008; Krause 2002; Weber et al. 2001). Thus, it can be concluded based on the results of this study and others that more forested and pasture land leads to less surface runoff; inversely, surface runoff increases and ET decreases as the area of bare land and urban land increases.

Conclusions

This study of various land-use scenarios shows that the hydrological impact of extensive rare earth mining activities has significantly changed the water balance components of the Taojiang River basin. We used a historical and hypothetical scenario method based on a modeling approach, which is a widely accepted way to research how LUCC affects the main water balance components of the hydrological process. The established SWAT model duplicated the local hydrological phenomena well. The research confirms that SWAT can be used to assess the hydrological impacts of rare earth mining activities with satisfactory accuracy.

The study found that the water balance in this basin has degraded from 2005 to 2015. The rank of capacity to generate surface runoff of the four dominant land-use types was, from highest to lowest: rare earth bare land, urban land, pasture land, and forested land. Due to the relatively small area involved, the rare earth mining activities were not enough to significantly deteriorate the local hydrological cycle from 2005 to 2015; therefore protecting the forest should be considered as the top priority in the future to achieve sustainable development. In addition, urban land also exerts a great impact on the water balance. Considering that the expansion of the urban area and population is an inevitable trend, minimizing the loss of forested land and enhancing infiltration in the urban areas should be the top priorities to mitigate the stress of urban land on the hydrological cycle.

The results provide important references for the sustainable development of rare earth mining activities in the Taojiang River basin and other similar mining regions. Notice that water quality is also a key component of the total water environment and that this study only focused on water quantity. Future work need to research the influence of urban growth and rare earth mining activities on both water quantity and quality, and reappraise the total water environment impacts of rare earth mining activities on the Taojiang River basin.

Acknowledgements We are grateful for the financial support from the National Key Technology Research and Development Program of the Ministry of Science and Technology of China (No. 2012BAC11B07),

the Science and Technology for Public Wellbeing Program of the Ministry of Science and Technology of China (No. 2013GS360203), the Training Programs for Leading Talents by Talents 555 Technology of Gan Poyang Lake of China, the National Natural Science Foundation of China (No. 51774153), the Cultivation of Excellent Doctoral Dissertations in Jiangxi University of Science and Technology (No. 3105500026), and the Subject of Jiangxi Education Department Science and Technology Planning of China (No. GJJ160595). We also thank the anonymous reviewers and editors for their helpful comments, which helped us to improve the quality of the paper.

References

Abbaspour KC, Yang J, Maximov I, Siber R, Bogner K, Mieleitner J, Zobrist J, Srinivasan R (2007) Modelling hydrology and water quality in the pre-alpine/alpine Thur watershed using SWAT. J Hydrol 333:413–430

Arabi M, Frankenberger JR, Engel BA, Arnold JG (2008) Representation of agricultural conservation practices with SWAT. Hydrol Process 22:3042–3055

Arnold JG, Allen PM (1999) Automated methods for estimating baseflow and ground water recharge from streamflow records. J Am Water Resour Assoc 35:411–424

Arnold JG, Moriasi DN, Gassman PW, Abbaspour KC, White MJ, Srinivasan R, Santhi C, Harmel RD, Van Griensven A, Van Liew MW, Kannan N, Jha MK (2012) SWAT: model use, calibration, and validation. Trans ASABE 55:1345–1352

Baker TJ, Miller SN (2013) Using the Soil and Water Assessment Tool (SWAT) to assess land use impact on water resources in an East African watershed. J Hydrol 486:100–111

Bao Z, Zhao Z (2008) Geochemistry of mineralization with exchangeable REY in the weathering crusts of granitic rocks in South China. Ore Geol Rev 33:519–535

Can T, Xiaoling C, Jianzhong L, Gassman PW, Sabine S, Josémiguel SP (2015) Assessing impacts of different land use scenarios on water budget of Fuhe River, China using SWAT model International. J Agric Biol Eng 8:95–109

Chengyou F, Dequan Z, Zailind Z, Song W (2012) Chronology of the tungsten feposits in southern Jiangxi Province, and episodes and zonation of the regional W-Sn mineralization-evidence from high-precision zircon U-Pb, molybdenite Re-Os and muscovite Ar-Ar ages. Acta Geol Sin Engl 86:555–567

Feyereisen GW, Strickland TC, Bosch DD, Sullivan DG (2007) Evaluation of SWAT manual calibration and input parameter sensitivity in the Little River watershed. T Asabe 50(3):843–855

Griensven AV, Meixner T, Grunwald S, Bishop T, Diluzio M, Srinivasan R (2006) A global sensitivity analysis tool for the parameters of multi-variable catchment models. J Hydrol 324:10–23

Gupta CK, Krishnamurthy N (2013) Extractive metallurgy of rare earths. Metall Rev 37:197–248

Gyamfi C, Ndambuki J, Salim R (2016) Hydrological responses to land use/cover changes in the Olifants Basin, South Africa. Water 8:588

Hu RZ, Zhou MF (2012) Multiple mesozoic mineralization events in south China—an introduction to the thematic issue. Miner Deposita 47:579–588

Hua G, Qi H, Tong J (2008) Annual and seasonal streamflow responses to climate and land-cover changes in the Poyang Lake basin, China. J Hydrol 355:106–122

Ishihara S, Hua R, Hoshino M, Murakami H (2010) REE abundance and REE minerals in granitic rocks in the Nanling Range, Jiangxi Province, southern China, and generation of the REE-rich weathered crust deposits. Resour Geol 58:355–372

Jayakrishnan R, Srinivasan R, Santhi C, Arnold JG (2005) Advances in the application of the SWAT model for water resources management. Hydrol Process 19:749–762

Jha MK, Arnold JG, Gassman PW (2007) Water quality modeling for the Raccoon River watershed using SWAT. Trans ASABE 50(2):479–493

Jordens A, Cheng YP, Waters KE (2013) A review of the beneficiation of rare earth element bearing minerals. Miner Eng 41:97–114

Jung YW, Oh DS, Kim M, Park JW (2010) Calibration of LEACHN model using LH-OAT sensitivity analysis. Nutr Cycl Agroecosyst 87:261–275

Kanazawa Y, Kamitani M (2006) Rare earth minerals and resources in the world. J Alloy Compd 37:1339–1343

Kaur R, Srinivasan R, Mishra K, Dutta D, Prasad D, Bansal G (2003) Assessment of a SWAT model for soil and water management in India. Land Use Water Resour Res 3:1–7

Krause P (2002) Quantifying the impact of land use changes on the water balance of large catchments using the J2000 model. Phys Chem Earth 27:663–673

Kruse NA, Bowman JR, Mackey AL, Mccament B, Johnson KS (2012) The lasting impacts of offline periods in lime dosed streams: a case study in Raccoon Creek, Ohio. Mine Water Environ 31:266–272

Kundu S, Khare D, Mondal A (2017) Past, present and future land use changes and their impact on water balance. J Environ Manag 197:582–596

Kushwaha A, Jain MK (2013) Hydrological simulation in a forest dominated watershed in Himalayan Region using SWAT Model. Int Ser Prog Water Resour Manag 27:3005–3023

Lai X, Cai M, Ren F, Xie M, Esaki T (2006) Assessment of rock mass characteristics and the excavation disturbed zone in the Lingxin Coal Mine beneath the Xitian river, China. Int J Rock Mech Min 43:572–581

Lee G, Shin Y, Jung Y (2014) Development of web-based RECESS model for estimating baseflow using SWAT. Sustainability 6:2357–2378

Li ZX, Li XH (2007) Formation of the 1300-km-wide intracontinental orogen and postorogenic magmatic province in Mesozoic South China: a flat-slab subduction model. Geology 35:179–182

Li P, Qian H, Wu J, Zhang Y, Zhang H (2013) Major Ion Chemistry of Shallow Groundwater in the Dongsheng Coalfield, Ordos Basin, China. Mine Water Environ 32:195–206

Li Z, Deng X, Wu F, Hasan SS (2015) Scenario analysis for water resources in response to land use change in the middle and upper reaches of the Heihe River basin. Sustainability 7:3086–3108

Li P, Tian R, Xue C, Wu J (2017) Progress, opportunities, and key fields for groundwater quality research under the impacts of human activities in China with a special focus on western China. Environ Sci Pollut Res 24:13224–13234

Mao J, Cheng Y, Chen M, Pirajno F (2013) Major types and time–space distribution of Mesozoic ore deposits in South China and their geodynamic settings. Miner Deposita 48:267–294

Maulana A, Yonezu K, Watanabe K (2014) Geochemistry of rare earth elements (REE) in the weathered crusts from the granitic rocks in Sulawesi Island, Indonesia. J Earth Sci 25:460–472

Mccarty JA, Haggard BE, Matlock MD, Pai N, Saraswat D (2016) Post-model validation of a deterministic watershed model using monitoring data. Trans ASABE 59:1–12

Mccullough CD, Etten EJBV (2011) Ecological restoration of novel lake districts: new approaches for new landscapes. Mine Water Environ 30:312–319

Moriasi DN, Gitau MW, Pai N, Daggupati P (2015) Hydrologic and water quality models: performance measures and evaluation criteria. Trans ASABE 58:1763–1785

Mudd GM (2007) An analysis of historic production trends in Australian base metal mining. Ore Geol Rev 32:227–261

Narsimlu B, Gosain AK, Chahar BR (2013) Assessment of future climate change impacts on water resources of upper Sind River basin, India using SWAT model. Int Ser Prog Water Resour Manag 27:3647–3662

Ng TL, Eheart JW, Cai X, Miguez F (2010) Modeling miscanthus in the soil and water assessment tool (SWAT) to simulate its water quality effects as a bioenergy crop. Environ Sci Technol 44:7138–7144

Palmer MA, Bernhardt ES, Schlesinger WH, Eshleman KN, Foufoulageorgiou E, Hendryx MS, Lemly AD, Likens GE, Loucks OL, Power ME, White PS, Wilcock PR (2010) Mountaintop mining consequences. Science 327:148–149

Poff NL, Zimmerman JKH (2010) Ecological responses to altered flow regimes: a literature review to inform the science and management of environmental flows. Freshw Biol 55:194–205

Ruan C, Jun T, Xianping L, Zhigao X, Zhengyan H (2012) The basic research on the weathered crust elution-deposited rare earth ores. Nonferr Met Sci Eng 3:1–13 **(in Chinese)**

Saha PP, Zeleke K (2015) Rainfall-runoff modelling for sustainable water resources management: SWAT model review in Australia. In: Sustainability of integrated water resources management: water governance, climate and ecohydrology. Springer International Publishing, Berlin, pp 563–578

Sanematsu K, Kon Y, Imai A, Watanabe K, Watanabe Y (2013) Geochemical and mineralogical characteristics of ion-adsorption type REE mineralization in Phuket, Thailand. Miner Deposita 48:437–451

Simandl GJ (2014) Geology and market-dependent significance of rare earth element resources. Miner Deposita 49:889–904

Tang X, Li M (2000) Landslide and its prevention of in situ leaching of ion-adsorption rare earth minerals. Met Mine 7:6–8 **(in Chinese)**

Volk M, Bosch D, Nangia V, Narasimhan B (2016) SWAT: agricultural water and nonpoint source pollution management at a watershed scale. Agric Water Manag 175:1–3

Weber A, Fohrer N, Möller D (2001) Long-term land use changes in a mesoscale watershed due to socio-economic factors—effects on landscape structures and functions. Ecol Model 140:125–140

White ED, Easton ZM, Fuka DR, Collick AS, Adgo E, McCartney M, Awulachew SB, Selassie YG, Steenhuis TS (2011) Development and application of a physically based landscape water balance in the SWAT model. Hydrol Process 25:915–925

Wu H, Chen B (2015) Evaluating uncertainty estimates in distributed hydrological modeling for the Wenjing River watershed in China by GLUE, SUFI-2, and ParaSol methods. Ecol Eng 76:110–121

Wu C, Huang D, Guo Z (1990) REE geochemistry in the weathered crust of granites, Longnan area, Jiangxi Province. Acta Geol Sin Engl 3:193–209

Wu J, Miao C, Zhang X, Yang T, Duan Q (2017) Detecting the quantitative hydrological response to changes in climate and human activities. Sci Total Envrion 586:328–337

Yang XJ, Lin A, Li XL, Wu Y, Zhou W, Chen Z (2013) China's ion-adsorption rare earth resources, mining consequences and preservation. Environ Dev 8:131–136

Zhang X, Srinivasan R, Arnold J, Izaurralde RC, Bosch D (2011) Simultaneous calibration of surface flow and baseflow simulations: a revisit of the SWAT model calibration framework. Hydrol Process 25:2313–2320

Zhang L, Kaixing W, Lingkang C, Ping Z, Huai O (2015) Overview of metallogenic features of ion-adsorption type REE deposits in southern Jiangxi Province. J Chin Soc Rare Earths 33(1):10–17 **(in Chinese)**